

Improving physics-informed neural network extrapolation via transfer learning and adaptive activation functions

A. Papastathopoulos-Katsaros^{1,2,†,*}
athanasios.papastathopoulos-katsaros@bcm.edu

Alexandra Stavrianidi^{3,†,*}
alexst@stanford.edu

Zhandong Liu^{1,2}
zhandong.liu@bcm.edu

¹Department of Pediatrics, Baylor College of Medicine, Houston TX 77030, USA

²Data Science Center, Jan and Dan Duncan Neurological Research Institute, Texas Children's Hospital, Houston TX 77030, USA

³Department of Mathematics, Stanford University, Stanford CA 94305, USA

[†]These authors contributed equally

^{*}Corresponding authors

Abstract

Physics-Informed Neural Networks (PINNs) are deep learning models that incorporate the governing physical laws of a system into the learning process, making them well-suited for solving complex scientific and engineering problems. Recently, PINNs have gained widespread attention as a powerful framework for combining physical principles with data-driven modeling to improve prediction accuracy. Despite their successes, however, PINNs often exhibit poor extrapolation performance outside the training domain and are highly sensitive to the choice of activation functions (AFs). In this paper, we introduce a transfer learning (TL) method to improve the extrapolation capability of PINNs. Our approach applies transfer learning (TL) within an extended training domain, using only a small number of carefully selected collocation points. Additionally, we propose an adaptive AF that takes the form of a linear combination of standard AFs, which improves both the robustness and accuracy of the model. Through a series of experiments, we demonstrate that our method achieves an average of 40% reduction in relative L_2 error and an average of 50% reduction in mean absolute error in the extrapolation domain, all without a significant increase in computational cost. The code is available at <https://github.com/LiuzLab/PINN-extrapolation>

1 Introduction

Physics-Informed Neural Networks (PINNs), introduced by Raissi et al. [20], are neural networks trained not only on data but also constrained by physical laws, expressed as partial differential equations (PDEs). By embedding physics as prior knowledge, PINNs restrict the space of admissible solutions and reduce overfitting. PINNs have been successful in various use cases, in fields such as fluid mechanics [5], medicine [14, 26], and earth science [3]. In this work, we focus on using PINNs as solvers for nonlinear PDEs.

We consider a nonlinear PDE of the form

$$u_t + \mathcal{N}(u) = 0, x \in D, t \in [0, T]$$

where $u(t, x)$ denotes the latent solution, \mathcal{N} denotes a nonlinear differential operator, D is the spatial domain and T is the final time. To ensure a well-posed problem, an initial condition is prescribed for u at $t = 0$, along with boundary conditions on ∂D . The mean squared error loss function of the neural network is given by

$$MSE = \frac{w_u}{N_u} \sum_{i=1}^{N_u} |u(t_u^i, x_u^i) - u^i|^2 + \frac{w_f}{N_f} \sum_{i=1}^{N_f} |u_t(t_f^i, x_f^i) + \mathcal{N}(u)(t_f^i, x_f^i)|^2$$

where $\{t_u^i, x_u^i, u^i\}_{i=1}^{N_u}$ denote the initial and boundary data prescribed to the problem and $\{t_f^i, x_f^i\}_{i=1}^{N_f}$ denote the collocation points in the domain where the PDE is enforced. The weights w_u and w_f reflect our trust in the data and the PDE, respectively.

Although PINNs require substantially less computational resources than finite elements methods [7, 26], are mesh-free, and easily programmed, they perform poorly in extrapolation tasks [8, 12] which assess their performance on test data $\{(t_{\text{test}}^i, x_{\text{test}}^i)\} \subset (T_{\text{train}}, T] \times D$, where $T > T_{\text{train}}$. In this paper, we propose a transfer-learning method that reduces the L_2 extrapolation error by 40% on average and the mean absolute extrapolation error by 50% on average across several benchmarks, including the Allen–Cahn (AC), Korteweg–de Vries (KdV), and Burgers equations.

2 Related Work

The original PINN architecture [20] uses the tanh activation function (AF) in all the layers. However, the performance of PINNs is strongly influenced by the choice of AF [1, 9, 15, 22], and selecting AF that reflect the functional form of the solution has been shown to improve performance. In [1], the authors use components of the PDE problem at hand (e.g., the PDE coefficients, the initial condition, analytical solutions in lower dimensions), while in [15], the authors propose using $x + \sin^2(x)$ to learn periodic functions. In [9] and [22], the authors introduce adaptive approaches. Following the ABU-PINN (Adaptive Blending Unit) method [22], one can take a linear combination of standard AFs (GELU, ELU, sigmoid, tanh, sin, exp, Softplus, and Swish) with adaptive weights and adaptive slopes as the AF f :

$$f(x) = \sum_{i=1}^N G(\alpha_i) \sigma_i(\beta_i x)$$

where $\sigma_i(\cdot)$, α_i , β_i denote the candidate AF, the learnable weight parameters, and the learnable scaling factors (adaptive slopes) respectively. The gate function $G(\cdot)$ is softmax, $G(\alpha_i) = \exp(\alpha_i) / \sum_{j=1}^N \exp(\alpha_j)$, so the search space is the convex hull of the set of candidate AF. In the rest of the paper, we will refer to these as ABU-PINN combinations.

The performance of the PINN also depends strongly on the selection of collocation points and the choice of the weights w_u and w_f . As demonstrated in prior works [24, 25], adaptively sampling collocation points from regions that exhibit large PDE residuals during training can substantially improve accuracy.

Different PDEs have different generalization capabilities [23], as equations with a higher time derivative $|u_t|$ exhibit more variance in the time domain. For some PDEs, the extrapolation error increases exponentially fast as one moves away from the training domain [8]. In [12], the authors propose a method that adjusts the gradient descent vector update to always point in a direction that reduces the PDE loss error during training. However, this is ineffective when the initial and boundary conditions are imposed as hard constraints to accelerate training [2], as the loss function only includes the PDE residual.

Motivated by these considerations, we incorporate the initial and boundary conditions as hard constraints and propose a transfer-learning (TL) method to deal with the extrapolation issue, in which the AF selection plays a crucial role. By retraining only the final layer of the network on a small set of carefully selected collocation points in the validation region and learning an optimal linear combination of AF, we improve the extrapolation performance substantially for several benchmarks on the Allen–Cahn (AC), Korteweg–de Vries (KdV), and Burgers equations. We achieve an average reduction of 40% for the L_2 and of 50% for the mean absolute extrapolation error.

By fine-tuning only the parameters of the final layer and those of the adaptive AF, we achieve this error reduction with a minimal computational cost (see Table 2). Fine-tuning only the final layer’s parameters is a common practice in transfer learning [6], and this approach is further supported by a layer-wise feature importance analysis we conducted for the AC equation (see Figure S16).

Prior transfer learning approaches for PINNs have primarily focused on parameter tuning and data reuse to achieve generalization across different physical systems. In these works, transfer learning is applied across tasks, from one PDE to another, to improve performance in forward problems [6, 10, 11, 17, 19, 21], and inverse problems [27]. In contrast, our method focuses on enhancing extrapolation performance for the same PDE in regions beyond the training domain. We also use a fundamentally different strategy that combines adaptive activation function design with localized retraining of only the final layer based on newly sampled high-loss collocation points from an intermediate region.

3 Method Description

We split our temporal domain into three segments: the training range, the validation range, and the testing range, i.e. $[0, T_{\text{train}}]$, $(T_{\text{train}}, T_{\text{val}}]$, and $(T_{\text{val}}, T_{\text{test}}]$, where $T = T_{\text{test}} > T_{\text{val}} > T_{\text{train}} > 0$. We use $T_{\text{train}} = \frac{T}{2}$, $T_{\text{val}} = \frac{4T}{5}$, and $T_{\text{test}} = T$. The final 20% of the temporal domain is reserved for extrapolation, as in [12] and other time-series prediction studies.

To enforce the initial and boundary conditions of the PDE as hard constraints, we perform a change of variables to the governing equations. This ensures that the constraints are satisfied exactly and eliminates the need to balance the data loss against the PDE loss using fine-tuned weights w_u and w_f .

Initial Training Phase

1. We begin by training the neural network on the domain $[0, T_{train}]$. The training is monitored using the L_2 error on the validation interval $[T_{train}, T_{val}]$, and early stopping is applied to prevent overfitting.
2. After early stopping, we assess the extrapolation performance by computing the L_2 error on the test interval $(T_{val}, T_{test}]$.
3. To investigate how different AF impact extrapolation, we fix the AF tanh in all the layers except the final one, where we experiment with different alternatives.

Transfer Learning (TL) Phase

1. After the initial training phase is complete, we freeze the weights of all the layers except the final one, which is a typical practice in TL.
2. We uniformly sample a relatively large number of collocation points from the interval $[0, T_{val})$ and calculate their respective loss in a forward pass of the network. We then select a very small number of those collocation points: the ones that led to the highest loss.
3. We retrain the network on those few collocation points, using the Adam optimizer, updating only the final layer's weights and the parameters of its AF. This helps refine the model's predictive ability in the extrapolation domain without disrupting earlier learned dynamics. We use L_2 regularization, which penalizes large deviations in the retrained weights by adding a term proportional to the square of their magnitude. Among several techniques to avoid catastrophic forgetting (including basic fine-tuning and Elastic Weight Consolidation [13]), L_2 regularization yielded the best performance, so we adopted it for all our experiments (see supplementary material section A).

4 Experimental Setup

4.1 Hyperparameter selection

We applied our method to the Allen–Cahn (AC), Korteweg–de Vries (KdV), and Burgers equations using neural networks composed of six layers with 32 neurons each. We use the L-BFGS optimizer [4], which ensures rapid convergence, paired with early-stopping. The network parameters are initialized using the Xavier scheme. For all equations, we use $8k$ uniformly sampled collocation points. For the KdV equation specifically, we also include 200 boundary points.

For the TL phase, we switch to the Adam optimizer for an additional 120 to 150 epochs, using a learning rate of $1e-3$ to $1e-2$. A total of 80 collocation points are selected for training in the transfer phase out of $4k$ uniformly sampled collocation points.

4.2 Sampling strategy

We experimented with varying the proportion of collocation points sampled in the training interval $[0, 0.5]$ and in the validation interval $(0.5, 0.8]$. Ultimately, we found that sampling exclusively from the validation interval produced the best results. Additionally, the existing mechanisms in our approach, including L_2 regularization, the chosen number of training epochs, and the step size adjustments during TL, were sufficient to prevent catastrophic forgetting. The corresponding results are presented in Figures S1, S6, S11.

4.3 Evaluation metrics

We consider the L_2 relative error and the mean absolute error (MAE) to evaluate the accuracy of the PINN solutions, defined as follows:

$$L_2 \text{ error} = \frac{\sqrt{\sum_{i=1}^N |u_\theta(x_i, t_i) - u(x_i, t_i)|^2}}{\sqrt{\sum_{i=1}^N |u(x_i, t_i)|^2}}$$

$$MAE = \frac{\sum_{i=1}^N |u_\theta(x_i, t_i) - u(x_i, t_i)|}{\sum_{i=1}^N |u(x_i, t_i)|}$$

where N is the number of test points, $u(x_i, t_i)$ is the reference solution at (x_i, t_i) , and $u_\theta(x_i, t_i)$ is the PINN solution at (x_i, t_i) . To measure the extrapolation error we take $\{(x_{\text{test}}^i, t_{\text{test}}^i)\}$, where x_{test}^i is sampled at a uniform spatial mesh grid in the spatial domain and t_{test}^i is on a uniform temporal grid in $(T_{val}, T_{test}]$. We use a temporal step size of 0.01 for Burgers, 0.005 for AC and KdV, and sample 400 collocation points at each time instant for AC, 600 for Burgers, and 500 for KdV.

To obtain the reference solution to the PDE, we used a finite difference method for spatial discretization combined with the implicit ODE solver `ode15s` in MATLAB. The second spatial derivative was approximated using a centered difference scheme, and the other terms were evaluated pointwise. To enforce the boundary conditions, the solution at the domain boundaries was explicitly set at every time step. The solver’s relative and absolute tolerances were set to $1\text{e-}6$ and $1\text{e-}8$, respectively, ensuring numerical stability and accuracy.

5 Experimental results

We benchmarked our method on three different equations: Allen-Cahn (AC), Korteweg–de Vries (KdV), and the viscous Burgers equation. Each experiment was repeated ten times, and we report the average results. In all examples, the training domain was set to $[0, 0.5]$, the validation domain to $[0.5, 0.8]$ and the extrapolation domain to $[0.8, 1]$. As mentioned previously, we evaluated the extrapolation performance of different AFs in the final layer while all other layers used \tanh . The pool of candidate AFs for the final layer consists of:

tanh: The most commonly used AF for PINNs.

ABU-PINN from [22]: A linear combination of different AF including GELU, ELU, sigmoid, \tanh , \sin , \exp , Softplus, and Swish. We take adaptive linear combinations of at least three and up to six AF at a time. The use of softmax for weight normalization is maintained as in [22].

$x + \sin^2(x)$ from [15]: It has been shown to improve performance, potentially due to its semi-periodic component and its monotonicity.

Linear combinations of \tanh (lctanh): $\sum_{i=1}^n w_i \tanh(a_i x + b_i)$, where the coefficients a_i, b_i, w_i are optimized.

Linear combinations of \sin (lcsin): $\sum_{i=1}^n w_i \sin(a_i x + b_i)$, where the coefficients a_i, b_i, w_i are optimized.

Linear combinations of $x + \sin^2(x)$: $\sum_{i=1}^n (a_i x + b_i \sin^2(c_i x + d_i))$, where the coefficients a_i, b_i, c_i, d_i are optimized.

As noted in [22], each PDE tends to have a preferred AF; for example, \tanh performs best for the Allen–Cahn and viscous Burgers equations, while $x + \sin^2(x)$ is preferred for KdV. Building on this insight, we consider adaptive linear combinations of the preferred AF for each PDE (see supplementary material section D).

5.1 Allen-Cahn (AC) equation

The AC equation is given by

$$\begin{aligned} u_t - 0.0001u_{xx} + 5u^3 - 5u &= 0, \quad x \in [-1, 1], \quad t \in [0, 1], \\ u(0, x) &= x^2 \cos(\pi x), \quad u(-1, t) = u(1, t) = -1. \end{aligned}$$

We enforce the initial and boundary conditions as hard constraints by setting

$$u(t, x) = x^2 \cos(\pi x) + t(1 - x^2)v(t, x).$$

Then u automatically satisfies the initial and boundary conditions, and we only need to impose the PDE constraint on v (see supplementary material section B).

The best ABU-PINN was the combination of \tanh , GELU, and sigmoid. For lctanh and lcsin, the combination of three AF was shown to give the best results. Our findings are presented in Table 1. Overall, a linear combination of \tanh provided the best extrapolation accuracy while introducing a similar number of trainable parameters as other linear combinations.

Regarding the TL results, we plot the collocation points with the highest PDE loss (the ones chosen for training) in Figure S1. As expected, these points are predominantly concentrated towards the end of the temporal validation domain and around the two regions with the largest spatial discrepancies. We trained for 150 epochs and set the learning rate for the Adam optimizer to $5\text{e-}3$.

The performance of various AF with TL is summarized in Table 1. Despite using only a small number of collocation points and training for a limited number of epochs, our results demonstrate substantial improvements. Specifically, we reduced the L_2 error from 0.20 to 0.12 compared to the standard PINN model and the MAE error from 0.11 to 0.06. A benchmark of our method against the state-of-the-art methods of References [12, 16, 18] is presented in Table 2. The results show that our TL approach outperforms all other methods.

Figures S2, S3, S4, and S5 allow for a visual comparison of the model performance with and without TL, as well as the performance of the \tanh AF versus the best lctanh. The results are shown for two different timestamps, $t = 0.82$ and $t = 0.99$, which highlight the challenges of extrapolation due to the rapid spatial transitions that occur over time. As illustrated in the figures, it is evident that both TL and a well-chosen AF contribute significantly to the improvement of the extrapolation performance. Furthermore, errors tend to be larger at later timestamps (t), a finding that aligns with [8].

AF	L_2		MAE	
	Without TL	With TL	Without TL	With TL
tanh	0.20	0.17	0.11	0.09
$x + \sin^2(x)$	0.23	0.19	0.14	0.1
ABU-PINN	0.19	0.14	0.11	0.08
lctanh	0.16	0.12	0.09	0.06
lcsin	0.18	0.14	0.10	0.07

Table 1: Comparative analysis of L_2 and MAE errors for various AF applied to the AC equation, demonstrating the effectiveness of TL and of carefully selected AF. Results for lctanh, lcsin, and ABU-PINN correspond to the optimal linear combinations described in the main text.

Method	L_2 extrapolation error
lctanh w/o TL (ours)	0.16
lctanh w/ TL (ours)	0.12
SA-PINN [16]	0.18
w-s PINN [18]	0.14
DPM [12]	0.18

Table 2: Comparison of our methods with state-of-the-art approaches applied to the AC equation.

5.2 Korteweg–de Vries (KdV) equation

The KdV equation is given by

$$u_t + uu_x + 0.0025u_{xxx} = 0, \quad x \in [-1, 1], \quad t \in [0, 1],$$

$$u(0, x) = \cos(\pi x), \quad u(t, -1) = u(t, 1), \quad u_x(t, -1) = u_x(t, 1).$$

We enforce the initial condition as a hard constraint by setting

$$u(t, x) = \cos(\pi x) + tv(t, x)$$

Then u automatically satisfies the initial condition, and we only need to impose the PDE constraint and the boundary conditions on v (see supplementary material section B).

The best ABU-PINN was the combination of tanh, GELU, and sin. For lctanh and lcsin, the combination of three AFs yielded the best results, while the combination of two AFs achieved similar performance. Our findings are presented in Table 3. Overall, a linear combination of $x + \sin^2(x)$ with $n = 2$ provided the best extrapolation accuracy while introducing a similar number of trainable parameters as other linear combinations. As is the case for AC, we observe that the best adaptive linear combination is the linear combination of the single preferred AF, in this case, $x + \sin^2(x)$.

Regarding TL, we plot the collocation points with the highest PDE loss in Figure S6. We trained for 150 epochs and set the learning rate for the Adam optimizer to $5e-2$. The performance of the different AF with TL is summarized in Table 3. Our method reduced the L_2 error from 0.15 to 0.08 compared to the standard PINN model and the MAE error from 0.12 to 0.06. A benchmark of our method against the state-of-the-art method of Reference [18] can be found in Table 4. The results show that our TL approach outperforms the other method. Figures S7, S8, S9, and S10 present example calculations that compare model performance with and without TL, as well as the performance of the tanh AF versus the best $\text{lc}(x + \sin^2(x))$.

AF	L_2		MAE	
	Without TL	With TL	Without TL	With TL
tanh	0.15	0.13	0.12	0.10
$x + \sin^2(x)$	0.12	0.09	0.08	0.07
ABU-PINN	0.14	0.11	0.09	0.08
lctanh	0.14	0.12	0.11	0.09
lcsin	0.12	0.09	0.07	0.07
$\text{lc}(x + \sin^2(x))$	0.10	0.08	0.07	0.06

Table 3: Comparative analysis of L_2 and MAE errors for various AF applied to the KdV equation, demonstrating the effectiveness of TL and of carefully selected AF. Results for lctanh, lcsin, $\text{lc}(x + \sin^2(x))$, and ABU-PINN correspond to the optimal linear combinations described in the main text.

Method	L_2 extrapolation error
lc ($x + \sin^2(x)$) w/o TL (ours)	0.10
lc ($x + \sin^2(x)$) w/ TL (ours)	0.08
s-d PINN [18]	0.14

Table 4: Comparison of our methods with state-of-the-art approaches applied to the KdV equation.

5.3 Viscous Burgers’ equation

The viscous Burgers’ equation is given by

$$u_t + uu_x - \frac{0.01}{\pi} u_{xx} = 0, \quad x \in [-1, 1], \quad t \in [0, 1],$$

$$u(0, x) = -\sin(\pi x), \quad u(t, -1) = u(t, 1) = 0.$$

We enforce the initial and boundary conditions as hard constraints by setting

$$u(t, x) = -\sin(\pi x) + t(1 - x^2)v(t, x)$$

Then u automatically satisfies the initial and boundary conditions, and we only need to impose the PDE constraint on v .

The best ABU-PINN was the combination of tanh, GELU, sigmoid, and sin. For lctanh and lcsin, the combination of three AFs yielded the best results. Our results are summarized in Table 5. The linear combination of tanh provides the best extrapolation accuracy, and we see again that the adaptive linear combination that performs best is the linear combination of the single preferred AF.

We plot the collocation points with the highest PDE loss in Figure S11. As before, these points are predominantly concentrated towards the end of the temporal validation domain and around the region with the largest spatial discrepancies. We trained for 150 epochs and set the learning rate for the Adam optimizer to $5e-2$.

The performance of the various AF with TL is summarized in Table 5. We reduced the L_2 error from 0.09 to 0.06 compared to the standard PINN model, and the MAE error from 0.07 to 0.03. A benchmark of our method against the state-of-the-art methods of References [12, 16] can be found in Table 6. The results show that our approaches outperform all other methods. Figures S12, S13, S14, S15 present example calculations that compare model performance with and without TL, as well as the performance of the tanh AF versus the best lctanh.

AF	L_2		MAE	
	Without TL	With TL	Without TL	With TL
tanh	0.09	0.08	0.07	0.06
$x + \sin^2(x)$	0.08	0.08	0.04	0.03
ABU-PINN	0.11	0.09	0.04	0.03
lctanh	0.07	0.06	0.04	0.03
lcsin	0.10	0.07	0.04	0.04

Table 5: Comparative analysis of L_2 and MAE errors for various AF applied to the Burgers’ equation, demonstrating the effectiveness of TL and of carefully selected AF. Results for lctanh, lcsin, and ABU-PINN correspond to the optimal linear combinations described in the main text.

Method	L_2 extrapolation error
lctanh w/o TL (ours)	0.07
lctanh w/ TL (ours)	0.06
SA-PINN [16]	0.08
DPM [12]	0.09

Table 6: Comparison of our methods with state-of-the-art approaches applied to the Burgers’ equation.

6 Conclusion

In this work, we introduced a transfer learning (TL) method paired with adaptive activation functions (AF) to improve the extrapolation performance of physics-informed neural networks (PINNs). Through a series of numerical experiments, we

demonstrated that our approach significantly outperforms the vanilla PINN while requiring minimal additional training cost and is also superior to three state-of-the-art methods. Our results highlight that both the choice of AF and the use of targeted TL within the validation region contribute to substantial gains. We evaluated our method on three partial differential equations (PDEs) and achieved an average of 40% L_2 error reduction and an average of 50% mean absolute error reduction in the extrapolation domain.

We observed across all tested PDEs that the points with the highest PDE loss were found in the validation region, primarily near the domain’s boundary. Selecting even a small number of such high-loss collocation points for the TL and implementing a regularization scheme to prevent catastrophic forgetting resulted in notable improvements in extrapolation performance.

Additionally, we found that an adaptive linear combination of the PDE-specific preferred AF outperformed combinations of other AF, including multiple diverse AFs. These results suggest that the key to improved extrapolation lies in the adaptability introduced by learnable AF weights and that increasing the diversity of AFs in the combination (as in ABU-PINN) is suboptimal.

However, our method was evaluated only on 1D PDEs over regular domains, and its scalability to more complex systems remains uncertain. In higher dimensions, collocation point selection becomes more critical, and enforcing boundary conditions as hard constraints on irregular domains may not be feasible. Applying our approach in such settings may require substantial adaptations and increased computational resources. Nonetheless, our method can still be applied in cases where real-world data is available, as our adaptive AF and TL approaches can still be implemented.

Acknowledgments

This work was supported by the National Institutes of Health (NIH) under grant number 5R01HG011795 and by the Cancer Prevention and Research Institute of Texas (CPRIT) under grant number RP240131. The authors also gratefully acknowledge the ICANN 2025 reviewers for their valuable feedback.

References

- [1] J. Abbasi and P.Ø. Andersen. Physical activation functions: An approach for more efficient induction of physics into physics-informed neural networks. *Neurocomputing* **608** (2024).
- [2] T. Alkhalifah and X. Huang. Direct Imaging Using Physics Informed Neural Networks. *2022 IEEE International Conference on Image Processing (ICIP)* (2022), 2781–2785.
- [3] P. Borate et al. Using a physics-informed neural network and fault zone acoustic monitoring to predict lab earthquakes. *Nat. Commun.* **14** (2023).
- [4] R.H. Byrd et al. A Limited Memory Algorithm for Bound Constrained Optimization. *SIAM J. Sci. Comput.* **16** (1995), pp. 1190–1208.
- [5] S. Cai et al. Physics-informed neural networks for fluid mechanics: a review. *Acta Mech. Sin.* **37** (2021), pp. 1727–1738.
- [6] S. Desai et al. One-Shot Transfer Learning of Physics-Informed Neural Networks. *arXiv e-prints* 2110.11286v2 (2021).
- [7] S.A. Faroughi et al. Physics-Informed Neural Networks with Periodic Activation Functions for Solute Transport in Heterogeneous Porous Media. *Mathematics* **12.1** (2024).
- [8] L. Fesser, L.D’Amico-Wong, and R. Qiu. Understanding and mitigating extrapolation failures in physics-informed neural networks. *arXiv e-prints* 2306.09478 (2023).
- [9] A. Jagtap, K. Kawaguchi, and G. Karniadakis. Locally adaptive activation functions with slope recovery for deep and physics-informed neural networks. *Proc. R. Soc. A* (2020).
- [10] D. Jalili et al. Transfer learning through physics-informed neural networks for bubble growth in superheated liquid domains. *Int. J. Heat Mass Transf.* **232** (2024), pp. 125940.
- [11] T. Kapoor et al. Transfer learning for improved generalizability in causal physics-informed neural networks for beam simulations. *Eng. Appl. Artif. Intell.* **133** (2024), pp. 108085.
- [12] J. Kim et al. DPM:A Novel Training Method for Physics-Informed Neural Networks in Extrapolation. *35th AAAI Conference on Artificial Intelligence* (2021), 8146–8154.
- [13] J. Kirkpatrick et al. Overcoming catastrophic forgetting in neural networks. *Proc. Natl. Acad. Sci.* **114** (2016), pp. 3521–3526.
- [14] G. Kissas et al. Machine learning in cardiovascular flows modeling: Predicting arterial blood pressure from non-invasive 4D flow MRI data using physics-informed neural networks. *Comput. Methods Appl. Mech. Eng.* **358** (2020), pp. 112623.
- [15] Z. Liu, H. Tilman, and U. Masahito. Neural Networks Fail to Learn Periodic Functions and How to Fix It. *Adv. Neural Inf. Process. Syst.* **33** (2020).

- [16] L. D. McClenny and U.M. Braga-Neto. Self-adaptive physics-informed neural networks. *Journal of Computational Physics* **474** (2023), 111722.
- [17] A. H. Mustajab et al. Physics-Informed Neural Networks for High-Frequency and Multi-Scale Problems Using Transfer Learning. *Appl. Sci.* **14.8** (2024), pp. 3204.
- [18] M. Penwarden et al. A unified scalable framework for causal sweeping strategies for physics-informed neural networks (PINNs) and their temporal decompositions. *J. Comput. Phys.* **493** (2023).
- [19] K. Prantikos et al. Physics-informed neural network with transfer learning (TL-PINN) based on domain similarity measure for prediction of nuclear reactor transients. *Sci Rep* **13.1** (2023), pp. 16840.
- [20] M. Raissi, P. Perdikaris, and G.E. Karniadakis. Physics-informed neural networks: A deep learning framework for solving forward and inverse problems involving nonlinear partial differential equations. *J. Comput. Phys.* **378** (2019), pp. 686–707.
- [21] A. Shima et al. Modeling unobserved geothermal structures using a physics-informed neural network with transfer learning of prior knowledge. *Geotherm Energy* **12.1** (2024), pp. 38.
- [22] Honghui Wang et al. Learning Specialized Activation Functions for Physics-informed Neural Networks. *arXiv e-prints* 2308.04073 (2023).
- [23] Y. Wang, Y. Yao, and Z. Gao. An extrapolation-driven network architecture for physics-informed deep learning. *Neural Netw.* **183** (2025), pp. 106998.
- [24] C.L. Wight and J. Zhao. Solving Allen-Cahn and Cahn-Hilliard equations using the adaptive physics informed neural networks. *Commun. Comput. Phys.* **29** (2021), pp. 930–954.
- [25] C. Wu et al. A comprehensive study of non-adaptive and residual-based adaptive sampling for physics-informed neural networks. *Comput. Methods Appl. Mech. Eng.* **403** (2023), pp. 115671.
- [26] B. Zapf et al. Investigating molecular transport in the human brain from MRI with physics-informed neural networks. *Sci. Rep.* **12** (2022).
- [27] J. Zhu, Y. Xue, and Z. Liu. A transfer learning enhanced physics-informed neural network for parameter identification in soft materials. *Appl. Math. Mech.-Engl. Ed.* **45.10** (2024), pp. 1685–1704.

Supplementary materials

A Comparison of TL Methods

In this study, we examined three TL methods: vanilla TL, L_2 regularization, and Elastic Weight Consolidation (EWC) [13]. We implemented all three methods by adjusting only the parameters of the final layer of the network while keeping all hyperparameters the same for a fair comparison.

In the vanilla model, the neural network was trained using standard backpropagation without any additional regularization terms. This approach serves as a baseline for comparing the effectiveness of advanced regularization techniques.

L_2 regularization modifies the loss function to prevent the model from overfitting to the new collocation points and avoid catastrophic forgetting, aiming to improve its generalizability. The modified loss function is given by:

$$\mathcal{L}(\theta) = \mathcal{L}_{\text{new}}(\theta) + \lambda \sum_i \theta_i^2$$

where:

- $\mathcal{L}(\theta)$ is the total loss function,
- $\mathcal{L}_{\text{new}}(\theta)$ is the loss function for the new task, measuring the loss at the new collocation points,
- θ represents the parameters of the neural network,
- θ_i is the i -th parameter of the model,
- λ is a regularization parameter that controls the trade-off between fitting the data well and keeping the model weights small to avoid overfitting. We experimented with multiple values and found 0.01 to be optimal across all the PDEs we tested.

EWC is a method specifically designed to mitigate catastrophic forgetting during the TL process. To the best of our knowledge, it has not been tested on PINNs. It adds a penalty to the loss function, which is proportional to the square of the difference between the current and previous weights, scaled by the importance of the weights to previous tasks. Mathematically, it is given by:

$$\mathcal{L}(\theta) = \mathcal{L}_{\text{new}}(\theta) + \sum_i \frac{\lambda}{2} F_i (\theta_i - \theta_i^*)^2$$

where:

- $\mathcal{L}(\theta)$ is the total loss function,
- $\mathcal{L}_{\text{new}}(\theta)$ is the loss function for the new task, measuring the loss at the new collocation points,
- θ represents the parameters of the neural network,
- θ_i is the current value of the i -th parameter,
- θ_i^* is the value of the i -th parameter after training on previous tasks,
- F_i is the diagonal element of the Fisher Information Matrix for the i -th parameter, indicating its importance to previous tasks,
- λ is a hyperparameter that controls the strength of the regularization. We experimented with multiple values and found 0.001 to be optimal across all the PDEs we tested.

Table S1 summarizes the performance of each TL method on the AC equation, noting the increase of the L_2 error in the training domain and the decrease of L_2 error in the extrapolation domain (denoted by catastrophic forgetting rate and extrapolation error reduction, respectively). We used the ABU-PINN AF in the final layer, i.e. an adaptive linear combination of tanh, GELU, and sigmoid. The evaluation metrics consist of the relative L_2 error and the mean absolute error (MAE). Surprisingly, our findings reveal that EWC performs the worst, while the vanilla TL and the L_2 regularization method exhibit similar results. Notably, L_2 regularization presented an advantage, so we included it in all our experiments.

B Experimental results

B1 Allen-Cahn equation

The AC equation is given by

$$\begin{aligned} u_t - 0.0001u_{xx} + 5u^3 - 5u &= 0, \quad x \in [-1, 1], \quad t \in [0, 1], \\ u(0, x) &= x^2 \cos(\pi x), \quad u(-1, t) = u(1, t) = -1. \end{aligned}$$

	Catastrophic forgetting rate within [0.0,0.8]		Extrap. error reduction within [0.8,1.0]	
TL method	L2 %	MAE %	L2 %	MAE %
Vanilla	7.7	38.7	36.9	43.2
L2 reg.	5.2	64.7	40.1	43.8
EWC	15.6	68.3	11.4	15.6

Table S 1: Summary of catastrophic forgetting and extrapolation performance for the AC equation using the ABU-PINN AF across different TL methods.

We enforce the initial and boundary conditions as hard constraints by setting

$$u(t, x) = x^2 \cos(\pi x) + t (1 - x^2) v(t, x).$$

Then u automatically satisfies the initial and boundary conditions, and we only need to impose the PDE constraint on v , which satisfies the equation

$$\begin{aligned} & (1 - x^2)v + t(1 - x^2)v_t \\ & - 0.0001 [2 \cos(\pi x) - 4\pi x \sin(\pi x) - \pi^2 x^2 \cos(\pi x) + t(-2v - 4xv_x + (1 - x^2)v_{xx})] \\ & + 5(x^2 \cos(\pi x) + t(1 - x^2)v(t, x))^3 - 5(x^2 \cos(\pi x) + t(1 - x^2)v(t, x)) = 0 \end{aligned}$$

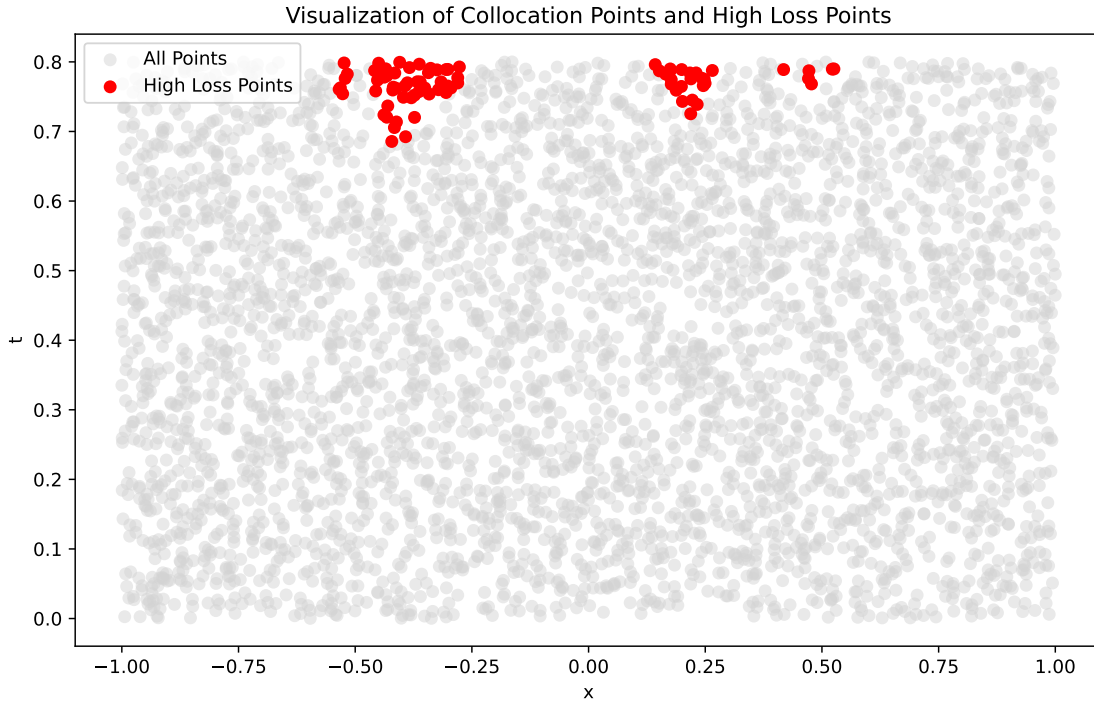
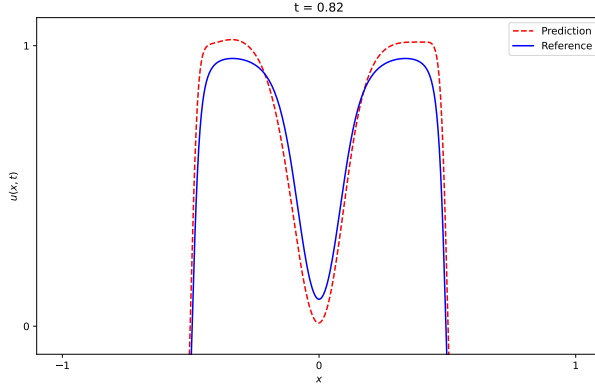
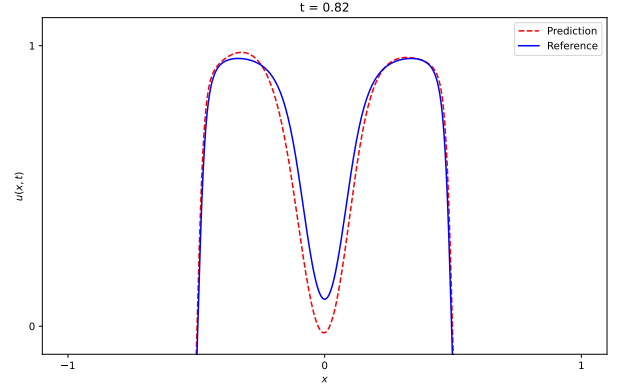


Figure S 1: The collocation points with the highest PDE loss for the AC equation are concentrated near the end of the temporal validation domain and around the regions of largest discrepancy in the spatial domain.

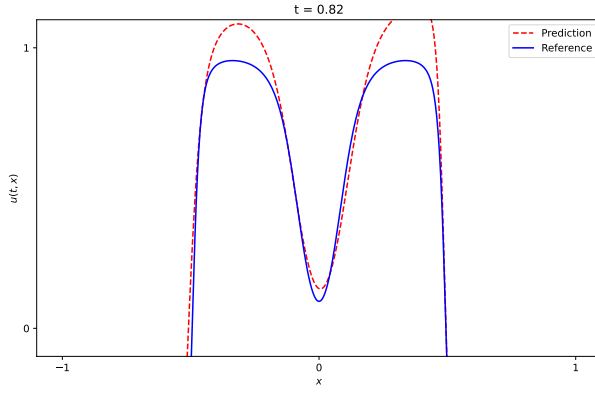


(a) Without TL

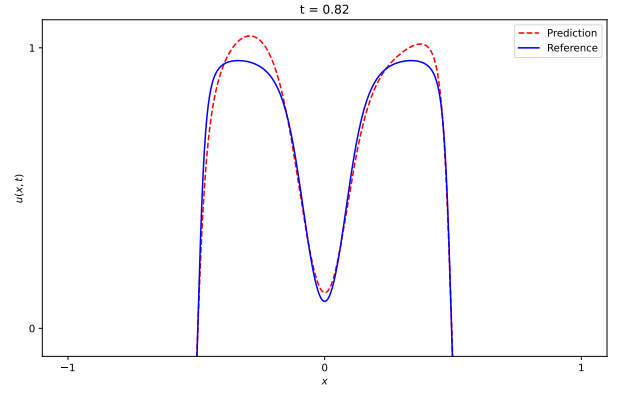


(b) With TL

Figure S 2: Comparison of solutions at $t = 0.82$ for the AC equation, with and without TL. Both subfigures display the reference solution alongside the PINN-predicted solution, using the lctanh AF in both cases.

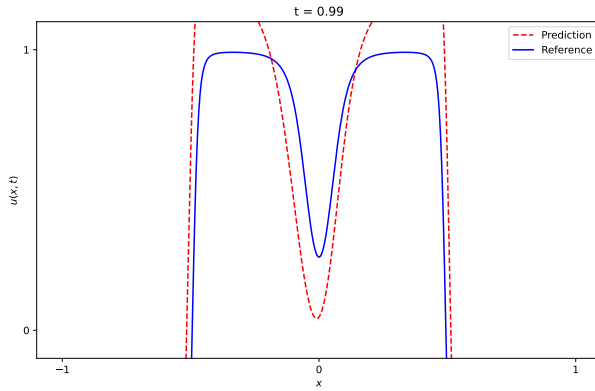


(a) tanh

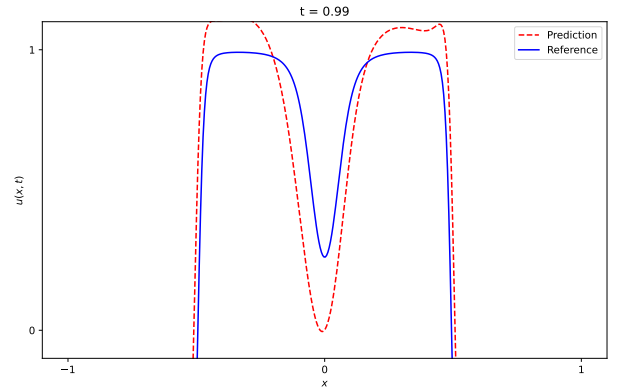


(b) lctanh

Figure S 3: Comparison of solutions at $t = 0.82$ for the AC equation, generated with \tanh and lctanh AF. Both subfigures display the reference solution alongside the PINN-predicted solution. No TL is used.

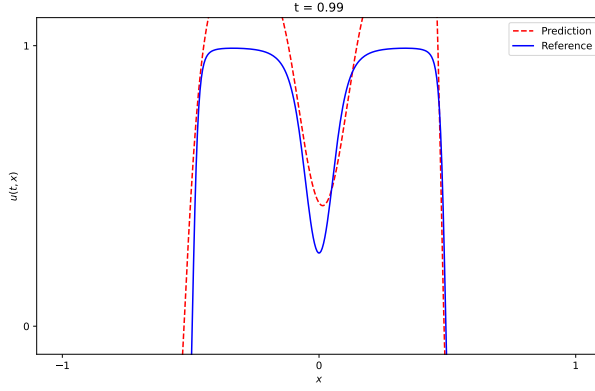


(a) Without TL

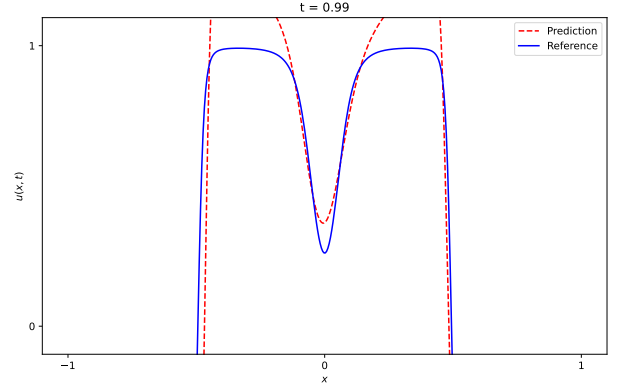


(b) With TL

Figure S 4: Comparison of solutions at $t = 0.99$ for the AC equation, with and without TL. Both subfigures display the reference solution alongside the PINN-predicted solution, using the lctanh AF in both cases.



(a) tanh



(b) lctanh

Figure S 5: Comparison of solutions at $t = 0.99$ for the AC equation, generated with tanh and lctanh AF. Both subfigures display the reference solution alongside the PINN-predicted solution. No TL is used.

B2 KdV equation

The KdV equation is given by

$$\begin{aligned} u_t + uu_x + 0.0025u_{xxx} &= 0, \quad x \in [-1, 1], \quad t \in [0, 1], \\ u(0, x) &= \cos(\pi x), \quad u(t, -1) = u(t, 1), \quad u_x(t, -1) = u_x(t, 1). \end{aligned}$$

We enforce the initial condition as a hard constraint by setting

$$u(t, x) = \cos(\pi x) + tv(t, x)$$

Then u automatically satisfies the initial condition, and we only need to impose the PDE constraint and the boundary conditions on v . Then v needs to satisfy

$$\begin{aligned} v + tv_t + (\cos(\pi x) + tv)(-\pi \sin(\pi x) + tv_x) + 0.0025(\pi^3 \sin(\pi x) + tv_{xxx}) &= 0 \\ v(t, -1) = v(t, 1), \quad v_x(t, -1) = v_x(t, 1). \end{aligned}$$

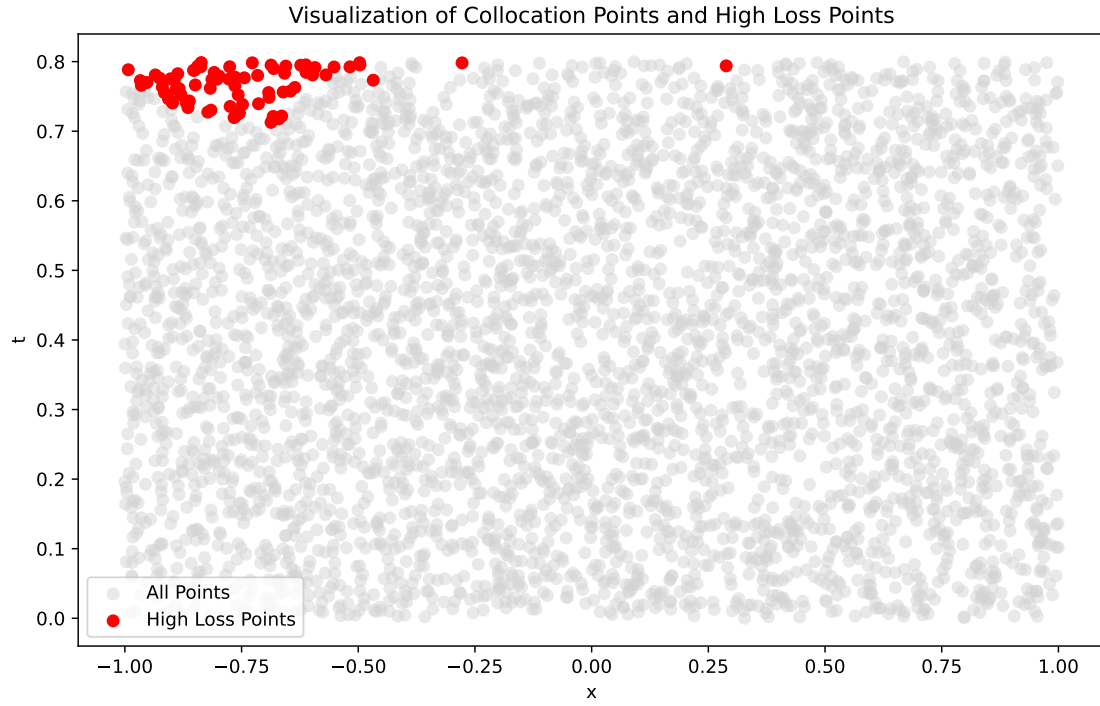
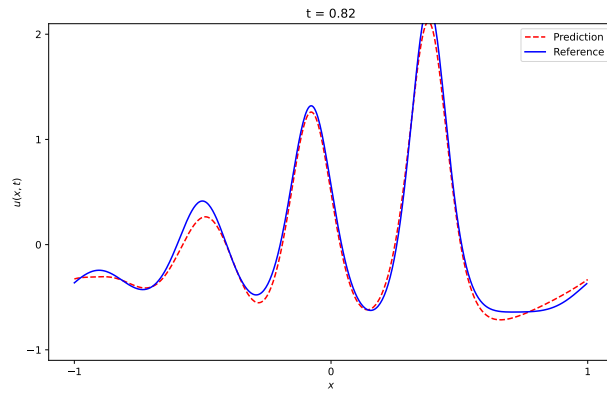
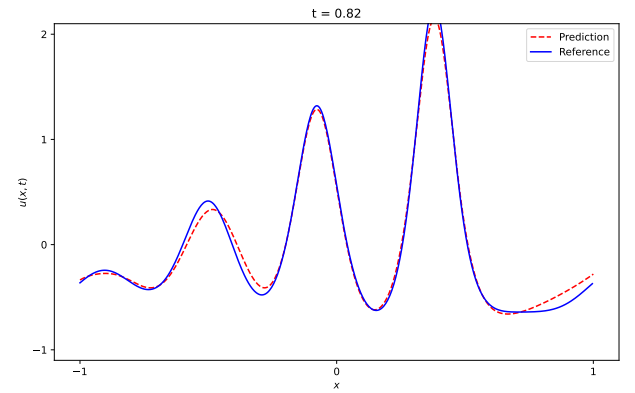


Figure S 6: The collocation points with the highest PDE loss for the KdV equation are concentrated near the end of the temporal validation domain and around the regions of largest discrepancy in the spatial domain.

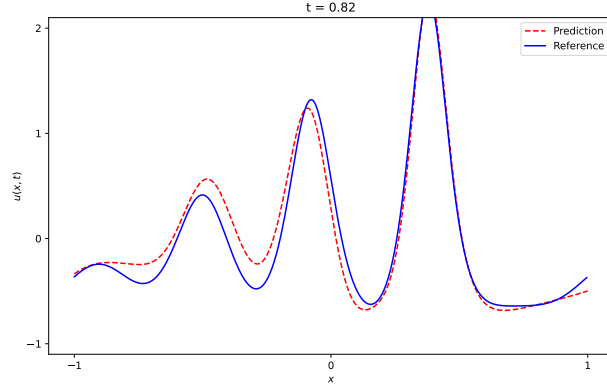


(a) Without TL

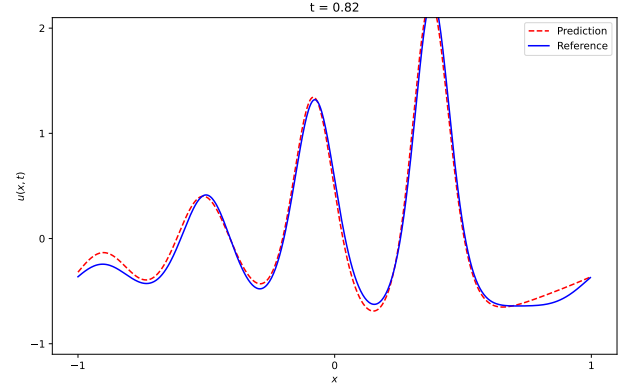


(b) With TL

Figure S 7: Comparison of solutions at $t = 0.82$ for the KdV equation, with and without TL. Both subfigures display the reference solution alongside the PINN-predicted solution, using the $\text{lc}(x + \sin^2(x))$ AF in both cases.

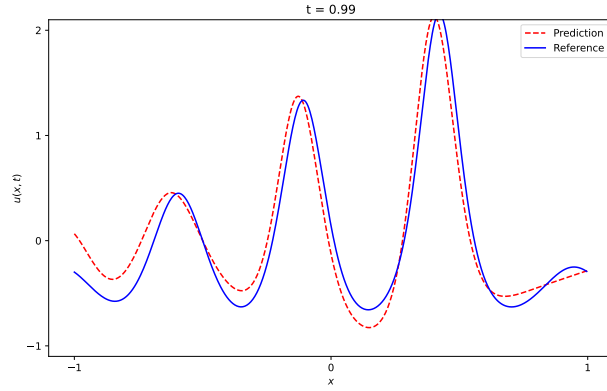


(a) tanh

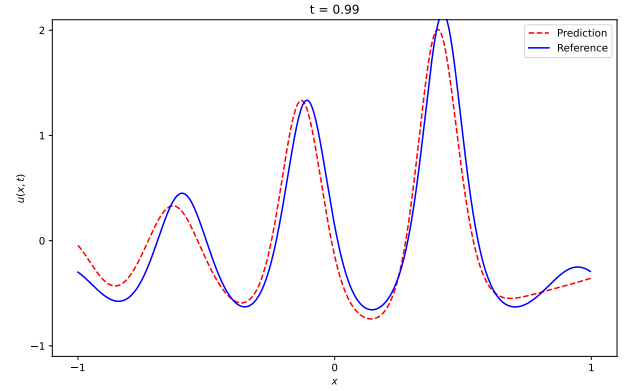


(b) $lc(x + \sin^2(x))$

Figure S 8: Comparison of solutions at $t = 0.82$ for the KdV equation, generated with tanh and $lc(x + \sin^2(x))$ AF. Both subfigures display the reference solution alongside the PINN-predicted solution. No TL is used.

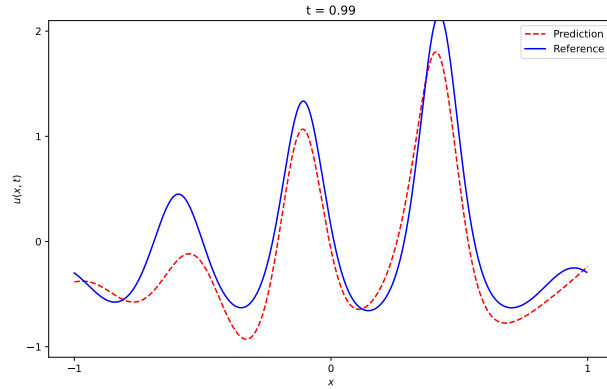


(a) Without TL

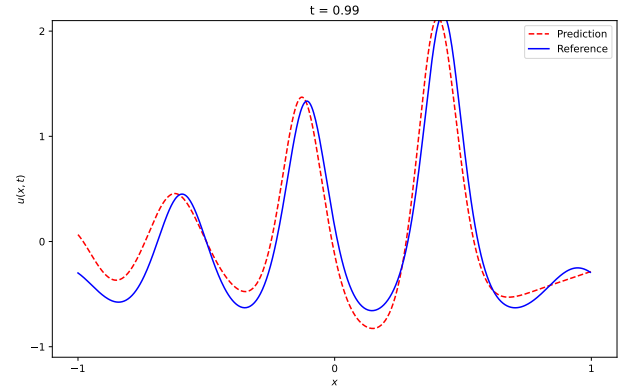


(b) With TL

Figure S 9: Comparison of solutions at $t = 0.99$ for the KdV equation, with and without TL. Both subfigures display the reference solution alongside the PINN-predicted solution, using the $lc(x + \sin^2(x))$ AF in both cases.



(a) tanh



(b) $lc(x + \sin^2(x))$

Figure S 10: Comparison of solutions at $t = 0.99$ for the KdV equation, generated with tanh and $lc(x + \sin^2(x))$ AF. Both subfigures display the reference solution alongside the PINN-predicted solution. No TL is used.

B3 Viscous Burgers' equation

The viscous Burgers' equation is given by

$$u_t + uu_x - \frac{0.01}{\pi} u_{xx} = 0, \quad x \in [-1, 1], \quad t \in [0, 1],$$

$$u(0, x) = -\sin(\pi x), \quad u(t, -1) = u(t, 1) = 0.$$

We enforce the initial and boundary conditions as hard constraints by setting

$$u(t, x) = -\sin(\pi x) + t(1 - x^2)v(t, x)$$

Then u automatically satisfies the initial and boundary conditions, and we only need to impose the PDE constraint on v . The equation for v is given by

$$(1 - x^2)v + t(1 - x^2)v_t + (-\sin(\pi x) + t(1 - x^2)v) (-\pi \cos(\pi x) + t(-2x)v + t(1 - x^2)v_x) - \frac{0.01}{\pi} (\pi^2 \sin(\pi x) - 2tv - 4xtv_x + t(1 - x^2)v_{xx}) = 0$$

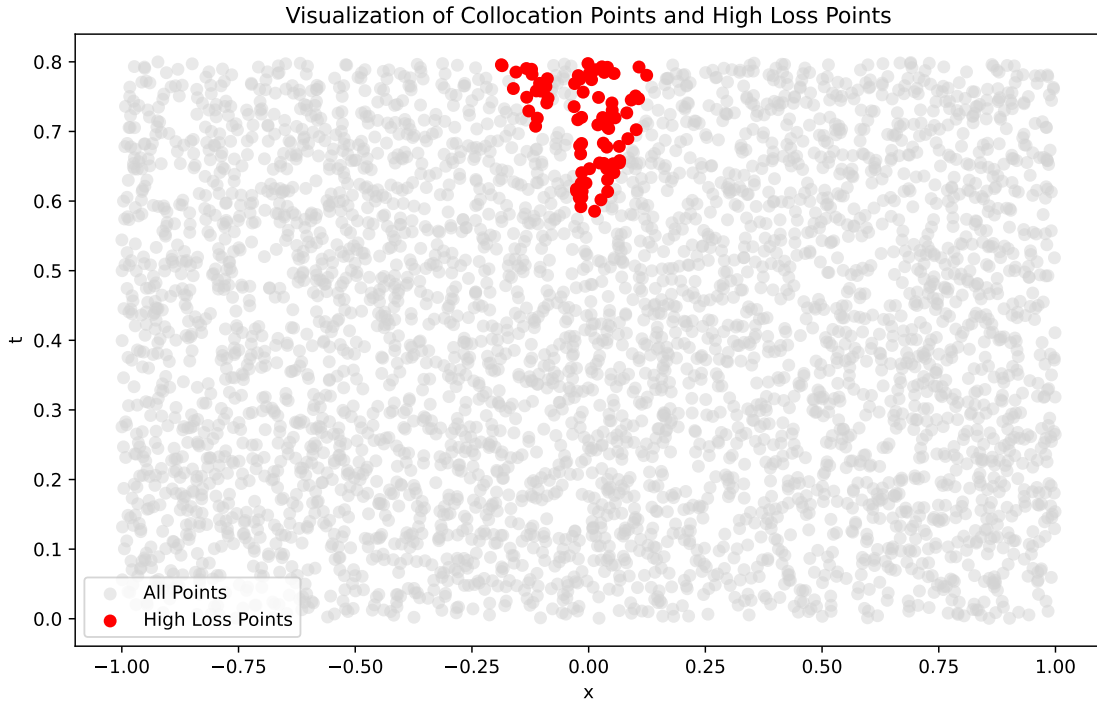
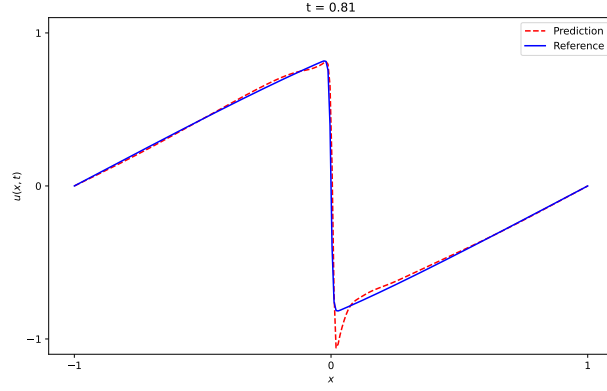
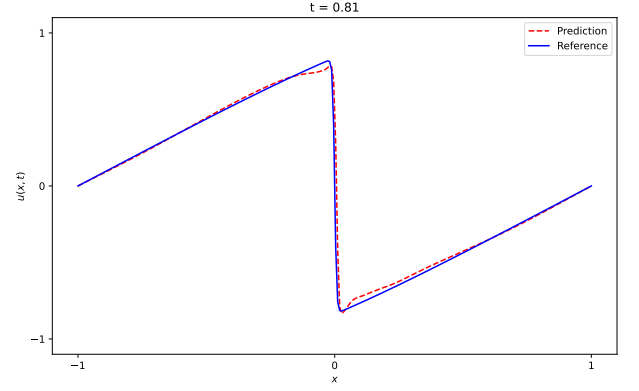


Figure S 11: The collocation points with the highest PDE loss for the Burgers' equation are concentrated near the end of the temporal validation domain and around the regions of largest discrepancy in the spatial domain.

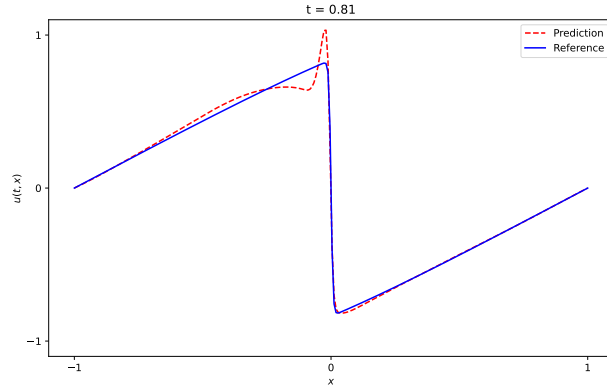


(a) Without TL

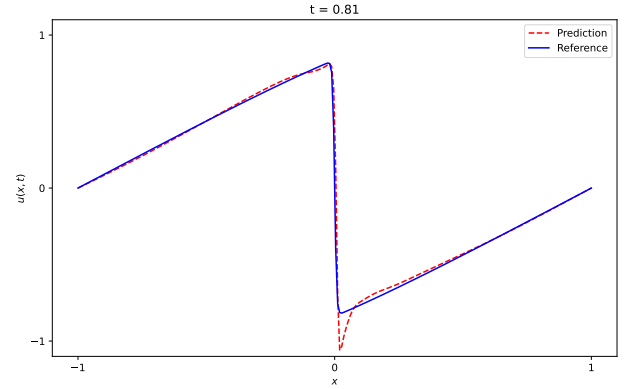


(b) With TL

Figure S 12: Comparison of solutions at $t = 0.81$ for the Burgers' equation, with and without TL. Both subfigures display the reference solution alongside the PINN-predicted solution, using the lctanh AF in both cases.

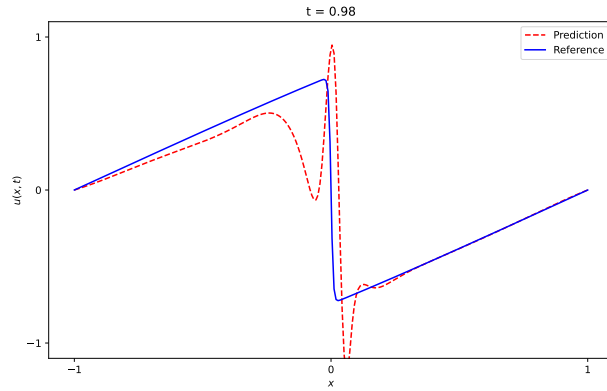


(a) tanh

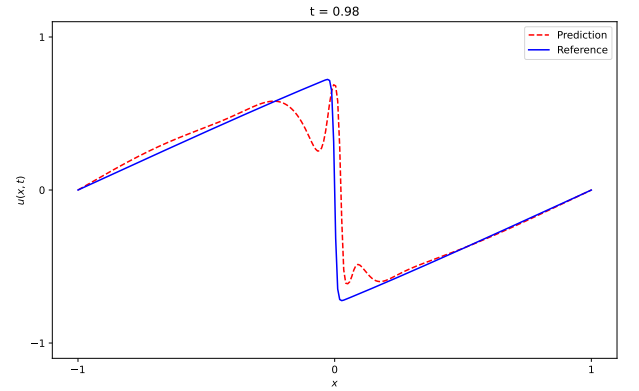


(b) lctanh

Figure S 13: Comparison of solutions at $t = 0.81$ for the Burgers equation, generated with tanh and lctanh AF. Both subfigures display the reference solution alongside the PINN-predicted solution. No TL is used.

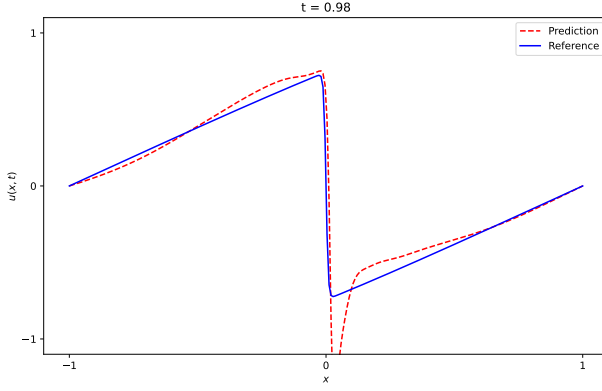


(a) Without TL

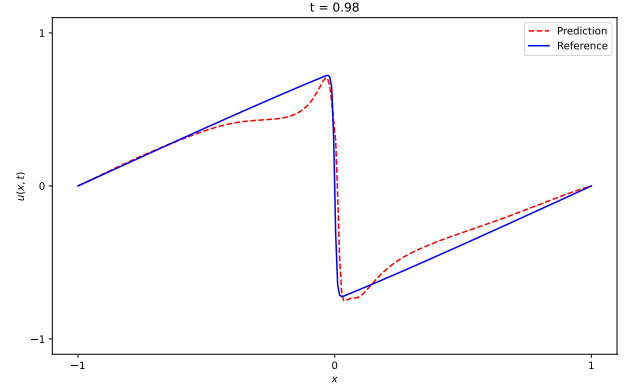


(b) With TL

Figure S 14: Comparison of solutions at $t = 0.98$ for the Burgers' equation, with and without TL. Both subfigures display the reference solution alongside the PINN-predicted solution, using the lctanh AF in both cases.



(a) tanh



(b) lctanh

Figure S 15: Comparison of solutions at $t = 0.98$ for the Burgers equation, generated with tanh and lctanh AF. Both subfigures display the reference solution alongside the PINN-predicted solution. No TL is used.

C Computational efficiency

We report the training times of our methods applied to the AC equation in Table S2 below.

Method	Training Time (min)
tanh w/o TL	51.6
lctanh w/o TL	58.3
tanh w/ TL	53.2
lctanh w/TL	60.7

Table S 2: Training time comparison for the vanilla PINN (tanh) and our improved AF PINN (lctanh), with and without TL, for the AC equation. The results show that modifying the activation function or incorporating TL has only a minimal effect on the training time.

D Methodological rationale: Final-layer fine-tuning and activation function selection

We introduce an adaptive AF only on the final layer, because, based on our findings (omitted), altering the AF throughout the network can negatively affect convergence and lead to training instability.

To further justify fine-tuning only the final layer, we performed a layer-wise analysis on the AC equation using the tanh AF. We first computed the L_2 norms of the weight and bias gradients, then took the logarithm of these norms and summed them together. We then visualized them in Figure S16. Our results reveal that the final three layers exhibit the largest values, indicating that these layers contribute most significantly to task-specific adaptation. This aligns with established transfer learning practices [6], where fine-tuning is typically performed on the final layers while earlier layers are frozen.

Regarding the AF selection, we experimented comparing ABU-PINN and lctanh for the AC equation. Our results show that, on average, lctanh achieved a training loss of $1e-5$ after 330 epochs, compared to 360 epochs for ABU-PINN, suggesting faster optimization. Additionally, lctanh began experiencing an increasing validation loss around epoch 720, while ABU-PINN did so around epoch 680, indicating that lctanh is less prone to overfitting. These findings provide evidence that the linear combination of tanh AFs can offer improved optimization and reduced overfitting compared to ABU-PINN, in addition to the PDE-specific reasons mentioned in the main text.

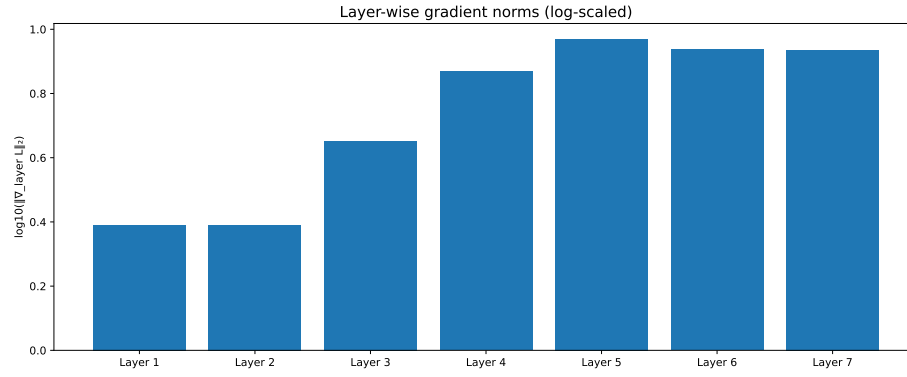


Figure S 16: Layer-wise gradient magnitudes (log-scaled L_2 norms) of the weight and bias terms, illustrating the contribution of each layer. The highest magnitudes are observed in the final hidden layers, suggesting their dominant role in the model's performance. Results are computed for the AC equation with the tanh AF.